RSC Sustainability

ROYAL SOCIETY OF CHEMISTRY

PAPER

View Article Online
View Journal | View Issue

Check for updates

Cite this: *RSC Sustainability*, 2025, **3**, 4029

Eco-sustainable magnetic polymer composites using recycled and rare-earth-free hard magnetic fillers†

Ayda Ghary Haghighat,[abc] Eider Matxinandiarena,[d] Manuela Zubitur,[de] Agurtzane Mugica,[d] Fulvio Bellato,[f] Anna M. Ferretti,[f] Alessandro Ponti,[f] Souad Ammar,[g] Maryam Abdolrahimi,[ab] Gaspare Varvaro,[b] Pierfrancesco Maltoni,[ab] Dario Cavallo,[a] Alexander Omelyanchik,*[ab] Alejandro J. Müller*[dh] and Davide Peddis*[ab]

Received 27th March 2025
Accepted 28th June 2025

DOI: 10.1039/d5su00222b

rsc.li/rscsus

Biodegradable polymer matrices, poly(ε-caprolactone) (PCL), and poly(butylene succinate-*ran*-butylene adipate) (PBSA) were used to fabricate magnetic composites with recycled NdFeB and rare earth-free lab-synthesized ferrite fillers ($SrFe_{12}O_{19}$ and $SrFe_{12}O_{19}$–$CoFe_2O_4$) across a wide filling range (1–90%). Results obtained by differential scanning calorimetry, polarized light optical microscopy, and phase contrast microscopy, indicated that the magnetic particles tend to aggregate, leading to bimodality in the crystallization process, which can be attributed to distinct regions of the composites with well-dispersed and aggregated particles. Notably, ferrite fillers exhibited lower magnetic anisotropy compared to NdFeB, enabling magnetic saturation at lower fields. These results demonstrate the potential of combining biodegradable polymers with sustainable magnetic fillers for eco-friendly circular economy applications.

Sustainability spotlight

This work addresses critical sustainability challenges by developing magnetic polymer composites that combine biodegradable matrices (PCL and PBSA) with either recycled neodymium magnets or rare-earth-free magnetic fillers. The research demonstrates a significant advancement toward circular economy principles in functional materials design. By successfully incorporating recycled NdFeB magnets and developing rare-earth-free alternatives, we present viable pathways to minimize environmental impacts associated with rare earth mining while maintaining functional magnetic properties. The integration of these fillers with biodegradable polymer matrices enhances the sustainability profile of these composites, as both PCL and PBSA can be produced from renewable resources. The systematic investigation of filler loading effects on thermal and magnetic properties provides essential knowledge for optimizing these materials for specific applications without compromising their environmental benefits. This research contributes to several UN Sustainable Development Goals: Responsible Consumption and Production (SDG 12) through the recycling of end-of-life permanent magnets; Industry, Innovation, and Infrastructure (SDG 9) through the development of new sustainable functional materials; and Climate Action (SDG 13) by promoting circular economy approaches that reduce environmental impacts associated with material extraction and processing.

1 Introduction

The development of polymer-based magnetic composites (PMCs) has garnered significant attention in recent years due to their potential applications in various fields, including biomedicine,[1] soft robotics,[2] and additive manufacturing.[3–5] The rapidly developing 3D printing technology has opened up new possibilities for processing materials, especially polymer

[a]*Università degli Studi di Genova, Dipartimento di Chimica e Chimica Industriale, nM²-Lab, Via Dodecaneso 31, 1-16146 Genova, Italy. E-mail: aleksander.omelianchik@ext.unige.it; davide.peddis@unige.it*

[b]*CNR, Istituto di Struttura della Materia, nM²-Lab, Monterotondo Scalo (Roma), 00015, Italy*

[c]*Università degli Studi Roma Tre, Dipartimento di Scienze, Via Ostiense 159, 00146 Rome, Italy*

[d]*POLYMAT and Department of Advanced Polymers and Materials: Physics, Chemistry and Technology, Faculty of Chemistry, University of the Basque Country UPV/EHU, Paseo Manuel de Lardizabal 3, Donostia, San Sebastián 20018, Spain. E-mail: alejandrojesus.muller@ehu.es*

[e]*Department of Chemical and Environmental Engineering, University of the Basque Country, UPV/EHU, Plaza Europa 1, 20018 Donostia-San Sebastián, Spain*

[f]*Consiglio Nazionale delle Ricerche, Istituto di Scienze e Tecnologie Chimiche "Giulio Natta", Via G. Fantoli 16/15, 20138 Milano, Italy*

[g]*Université Paris Cite, CNRS, ITODYS (UMR-7086), 15 rue JA de Baïf, 75205 Paris, France*

[h]*IKERBASQUE, Basque Foundation for Science, Plaza Euskadi 5, 48009 Bilbao, Spain*

† Electronic supplementary information (ESI) available. See DOI: https://doi.org/10.1039/d5su00222b

Open Access Article. Published on 15 2025. Downloaded on 02.11.2025 15:40:34.
This article is licensed under a Creative Commons Attribution-NonCommercial 3.0 Unported Licence.

Open Access Article. Published on 15 2025. Downloaded on 02.11.2025 15:40:34.
This article is licensed under a Creative Commons Attribution-NonCommercial 3.0 Unported Licence.

composites with magnetic inclusions, using the fused deposition modeling (FDM) method.[5] In this context, poly(lactic acid) (PLA), a standalone thermoplastic polymer, has attracted much interest due to its compatibility with 3D printing techniques and biodegradable nature.[6–14] However, other promising polymers, including poly(ε-caprolactone) (PCL)[15] and poly(butylene succinate-*ran*-butylene adipate) (PBSA),[16] remain relatively underexplored. PCL and PBSA are biodegradable polymers offering remarkable mechanical properties and significant environmental advantages.[15,17,18]

PCL, a semicrystalline polymer with a low melting temperature (T_m = 56–65 °C),[15] exhibits high flexibility and compatibility with various processing methods, including 3D printing. Its controlled biodegradation rate and biocompatibility make it a sustainable material for environmentally friendly applications.[15,19] PBSA is a copolymer of poly(butylene succinate) (PBS) with a melting temperature ($T_m \approx$ 84 °C)[20] lower than that of PBS but with comparable flexibility and processability.[17] PBSA benefits from improved enzymatic degradability due to its lower crystallinity compared with PBS.[17] Moreover, the PBS-based copolymers can be produced using bio-based renewable resources like sugarcane and corn.[18] Both PCL and PBS-based polymers are frequently blended with other biodegradable materials, such as PLA, to optimize mechanical and thermal properties, broadening their applicability in advanced composite designs.[9,18]

Incorporating magnetic micro- or nanoparticles (M(N)Ps) into polymer matrices significantly modifies the structural and thermal properties of the polymer matrix.[21] These effects are highly dependent on the composite processing method, the molecular mass of the polymer, and the surface functional groups of magnetic particles, leading to contradictory results in the literature. For instance, in ref. 9 it was reported that both T_m and the crystallization temperature (T_c) of PCL are not affected by the presence of Fe_3O_4 magnetic nanoparticles, while in ref. 22 the authors observed an opposite effect, with both T_m and T_c decreasing with increasing Fe_3O_4 nanoparticle content, likely due to a decreased chain mobility and crystallization ability caused by interactions between polymer chains and Fe_3O_4 *via* purposely introduced groups in PCL. Additional effects observed in polymer magnetic composites include a reduction in the size of PCL spherulites, accompanied by an increase in T_m when Fe_3O_4@graphene oxide nanocomposites are incorporated,[23] or changes in thermal stability, often accelerating degradation, driven by interactions between particles and polymer chains.[23,24] These findings highlight the complexity of such systems, underscoring the need for a systematic investigation, particularly in PCL and PBSA-based systems, to optimize their properties for advanced applications.

Beyond structural modifications, M(N)Ps impart unique functionalities, such as magnetic responsiveness.[21] By tailoring the type and concentration of M(N)Ps, these composites can be optimized for advanced applications, including 3D-printed magnets and intelligent devices.[9–13,25–28] PCL has been studied as electrospun fibrous[24] or 3D-printed[9] scaffolds for hyperthermia applications and magnetic-triggered actuators.[22] Fe_3O_4/PBSA composites have been investigated as magnetic actuators in soft robotics.[20] Research on these polymers remains limited, presenting an opportunity for novel investigations. Exploring biodegradable polymers in PMCs is crucial, as they offer unique attributes that complement those of more commonly studied materials.

It is worth mentioning that, to the best of our knowledge, in most cases involving PCL and PBSA, the magnetic properties of PMCs were controlled primarily by varying the content of simple iron oxides (magnetite Fe_3O_4 or maghemite γ-Fe_2O_3) nanoparticles. In contrast, PLA-based composites have been explored with a wider range of magnetic fillers, including cobalt ferrite $CoFe_2O_4$ (CFO),[6,8,13,29] zinc-substituted cobalt ferrite $Zn_{0.3}Co_{0.7}$-Fe_2O_4 and $CoFe_2O_4$ mixture,[6] and barium hexaferrites $BaFe_{12}O_{19}$.[6] This variability in composition enables the tuning of magnetic properties for targeted applications.

NdFeB stands out among various magnetic materials due to its exceptional magnetic properties, such as high saturation magnetization (M_S) and coercivity (H_C), making it the preferred choice for manufacturing high-performance permanent magnets.[30] However, the scarcity of rare earth elements (REEs), like neodymium, along with the environmental challenges associated with their extraction, has led to a growing demand for sustainable alternatives, and recycling of end-of-life permanent magnets emerged as a promising solution with significant potential for both the short and long term.[31–34] Although recycled magnetic materials generally underperform compared to solid NdFeB magnets in terms of energy product, PMCs offer significant advantages in terms of mechanical properties, corrosion resistance, and the ability to produce complex geometries, including micro-textured patterns.[21,26,27,35–38]

Another important category of magnetically hard materials is M-type hexaferrites ($MFe_{12}O_{19}$, where M = Ba or Sr).[39] These materials, which do not contain REEs, are known for their excellent chemical and oxidation resistance, low cost, high coercivity, and Curie temperature despite having relatively lower M_S. Their unique properties make hexaferrites attractive for applications where cost-effectiveness and moderate performance are desired, particularly in high-temperature environments.[39] Additionally, there has been an increasing interest in hexaferrite-based hard/soft exchange-coupled structures, combining the high anisotropy of the hard phase with the high saturation magnetization of the soft phase, resulting in enhanced magnetic performance for a variety of applications.[34,40,41]

In this variegated scenario, this work represents the first step to address the existing gap by selecting less commonly used, biodegradable PCL and PBSA polymers and incorporating three different types of magnetically hard particles: recycled NdFeB microparticles, REE-free lab-synthesized $SrFe_{12}O_{19}$ (SFO) nanoparticles and hard/soft $SrFe_{12}O_{19}$–$CoFe_2O_4$ (SFO-CFO) nanocomposites. The key novelty of this work lies in the use of biodegradable polymers and REE-free or recycled materials, aligning with the principles of circular economy and sustainable material design. The effects of incorporating these M(N)Ps into the polymer matrices, assessing mainly their influence on thermal properties were investigated. Additionally, the

© 2025 The Author(s). Published by the Royal Society of Chemistry

Open Access Article. Published on 15 2025. Downloaded on 02.11.2025 15:40:34.
This article is licensed under a Creative Commons Attribution-NonCommercial 3.0 Unported Licence.

tunability of the composite magnetic properties by varying the type and concentration of magnetic fillers was demonstrated.

2 Experimental

2.1 Materials

Strontium nitrate ($Sr(NO_3)_2$, Sigma-Aldrich), iron(III) nitrate nonahydrate ($Fe(NO_3)_3 \cdot 9H_2O$, Sigma-Aldrich), cobalt(II) nitrate hexahydrate ($Co(NO_3)_2 \cdot 6H_2O$), citric acid (Sigma-Aldrich), ammonia solution (30%, Sigma-Aldrich) were used as received. Deionized water was used in all synthetic procedures. Two commercially available biodegradable polymers, polycaprolactone (PCL, Perstorp Capa 6800, $M_w = 80\,000$ g mol^{-1}) and poly(butylene succinate-*ran*-butylene adipate) (PBSA, NaturePlast PBE 001, $M_w = 78\,000$ g mol^{-1}), were employed for the preparation of PMCs.

NdFeB microparticles employed in this work were donated by Dr Nerea Burgos from CEIT (University of Navarra, Spain). These microparticles were produced from different industrial waste sources by mixing NdFeB powder with an epoxy resin. Morpho-structural characterization of NdFeB microparticles is shown in the (ESI, Fig. S1–S3†). The X-ray diffraction pattern corresponds to the hexagonal $Nd_2Fe_{14}B$ crystalline structure. According to scanning electron microscopy, the NdFeB particles have spherical shapes with diameters in the range of 2–20 μm. Energy-dispersive X-ray spectroscopy (EDX) shows the copresence of B, Fe, and Nd.

2.2 Synthesis of SFO and SFO-CFO nanoparticles

SFO and SFO-CFO nanoparticles were synthesized using a modified sol–gel combustion method.[40,42] For SFO preparation, stoichiometric amounts of $Sr(NO_3)_2$ and $Fe(NO_3)_3 \cdot 9H_2O$ were dissolved in deionized water to achieve a Fe^{3+} concentration of 0.2 M. A 1 M citric acid solution was added as a chelating agent, maintaining a 1 : 1 molar ratio of total metals to citric acid. The pH of the solution was adjusted to 7 using 30% aq. NH_3. The mixture was then heated to 80 °C under constant stirring to form a gel, followed by rapid heating to 300 °C to induce flameless self-combustion. The resulting powder was ground and annealed at 950 °C under air for 3 hours.

A simultaneous bi-phasic approach was employed for the SFO-CFO synthesis. Precursors for CFO and SFO were separately prepared following the same initial steps as the SFO synthesis, then mixed in stoichiometric ratios to achieve 40 wt% SFO in the final composite. The combined solution underwent the same gel formation and combustion process, with the as-burnt powders annealed at 950 °C.

Structural and magnetic characterization of bare SFO and SFO-CFO magnetic nanoparticles are discussed in ref. 40. These samples are composed of interconnected particles forming aggregates: specifically, the morphology of SFO particles is characterized by a plate-like shape with a polycrystalline nature. The SFO-CFO system is characterized by an oriented growth relationship between SFO and CFO, with dislocations forming at the interface, indicating strong structural interactions.[43]

2.3 Characterization of the materials

Thermal properties were investigated by differential scanning calorimetry (TA DSC25). Calibration was done with indium and tin standards, and sealed aluminum pans of approximately 15 mg were used for the experiments in an ultra-high purity nitrogen atmosphere. Non-isothermal experiments were run in a temperature range between −40 and 80 °C for PCL PMCs and −40 and 130 °C for PBSA ones. 20 °C min^{-1} was employed as cooling and heating rates. First, thermal history is erased by keeping the samples for 3 min at 30 °C above the peak melting temperature of the polymer; samples were then cooled down, keeping them for 1 min at low temperatures to stabilize the system, and finally heated up at 20 °C min^{-1}.

Morphological properties were studied by an Olympus BX53M polarized light optical microscope (PLOM). It is equipped with a THMS600 Linkam hot stage, a liquid nitrogen cooling system for temperature control, and an SC50 Olympus camera for recording micrographs. Morphological changes were determined employing 20 °C min^{-1} as cooling and heating rates, in which samples were crystallized and melted on a glass slide with a thin glass coverslip on top. In addition, an Olympus BX53 phase-contrast microscope (PCM) was used to observe the morphology of samples at room temperature.

Field-dependent magnetization $M(H)$ loops were measured at 300 K using a vibrating sample magnetometer (VSM Model 10 – Microsense) in the magnetic field range ±2 T. The measurements were conducted to evaluate the magnetic response of the composites, including key parameters, such as coercivity ($\mu_0 H_C$), remanent magnetization (M_R), and magnetization measured at 2 T (M_{2T}).

3 Results and discussion

Commercial PCL and PBSA polymers were used to prepare PMCs with NdFeB, SFO, and SFO-CFO magnetic particles over a wide range of filler loading (C = 1–90%) for comparative analysis. The weight content (wt%) of magnetic particles was calculated using the (eqn S1). For PCL-based PMCs, the PCL homopolymer was weighed into aluminium pans, melted at 80 °C, and manually mixed with the desired amount of magnetic powder using a fine glass rod as a stirrer. The mixture was then cooled, and the total sample mass was recorded. Similarly, PBSA-based PMCs were prepared using the PBSA homopolymer, melted at 120 °C before being mixed with the magnetic particles using the same procedure. This experimental protocol was applied to prepare PCL and PBSA PMCs with all three types of magnetic particles (NdFeB, SFO, and SFO-CFO) to study the influence of particle type and concentration on the composite properties.

3.1 Thermal properties

The DSC cooling and heating scans of all the prepared PMCs exhibit similar behavior (Fig. S4–S9†), with the most significant differences observed in the low composition range of C = 1–10%. The cooling DSC scans within this range reveal a bimodal

Open Access Article. Published on 15 2025. Downloaded on 02.11.2025 15:40:34.
This article is licensed under a Creative Commons Attribution-NonCommercial 3.0 Unported Licence.

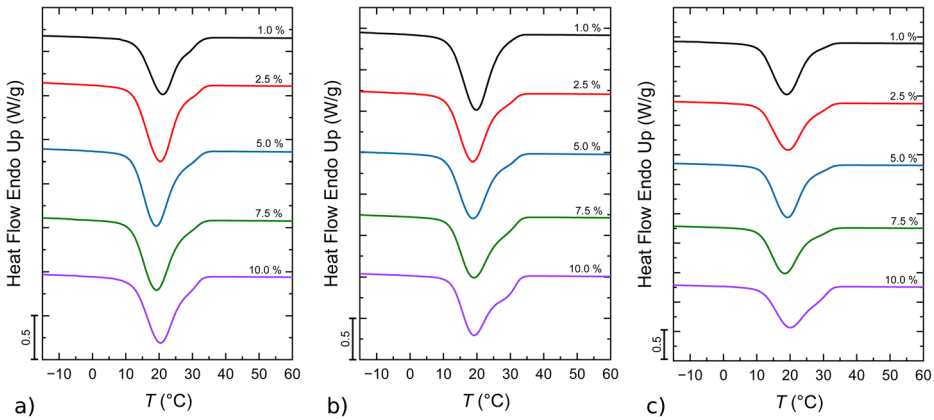

Fig. 1 DSC cooling curves at 20 °C min^{-1} of PCL composites with (a) NdFeB, (b) SFO, and (c) SFO-CFO magnetic micro- and nanoparticles in the composition range of 1–10%.

crystallization exotherm in some samples, suggesting poor dispersion of M(N)Ps (Fig. 1 and 2).

Fig. 1 shows DSC scans from the melt of selected samples. A main exothermic event corresponding to the PCL PMCs' crystallization is observed. The crystallization peaks contain a high-temperature shoulder at temperatures close to 30 °C or above, followed by the main peak. This is considered a bimodal crystallization, as two crystallization exotherms are overlapped. Fig. 2 shows the DSC cooling scans from the melt of PBSA composites. In this case, the bimodality of the crystallization exotherm is much more pronounced (with a high-temperature peak at approximately 40 °C and a low-temperature peak at approximately 10 °C). The exact values of all the calorimetric transitions recorded are reported in Tables S1–S12.† The higher temperature peaks (or shoulder) correspond to regions with better M(N)P dispersion, where the M(N)Ps effectively nucleate the polymer matrix. In contrast, the lower temperature peaks are associated with areas of M(N)P aggregation, where reduced surface contact with the polymer matrix hinders their nucleating effect.

Polymers crystallize by nucleation (or primary nucleation) and growth (or secondary nucleation, as crystals grow by successive nucleation on the previously formed primary nuclei) mechanism, where primary nuclei form and crystals can grow on them through secondary nucleation mechanisms. The nucleation of neat polymers is normally triggered by heterogeneities or impurities, like catalytic debris and others, *i.e.*, the so-called heterogeneous nucleation. The crystallization temperature upon cooling from the melt is proportional to the active heterogeneous nucleation density. The higher the crystallization temperature, the higher the nucleation density, which implies a more efficient nucleation process. Therefore, if a foreign substance, like a filler, is added to a polymer matrix, the crystallization temperature will only increase if the filler has a higher nucleating efficiency than the heterogeneities available within the polymer.[44,45]

The bimodality in the DSC crystallization exotherms is related to different primary nucleation effects. The nucleation of the filler occurs by interactions of the polymer chains and the exposed surface area of the fillers. When the dispersion is heterogeneous, the well-dispersed particles can cause the maximum nucleation effects, as their surface area is much higher in comparison with aggregates. The fact that the bimodality is due to nucleation effects and not to other possible reasons (like the crystallization of two polymorphs) is also proven by the DSC subsequent heating scans (Fig. S8 and S9†),

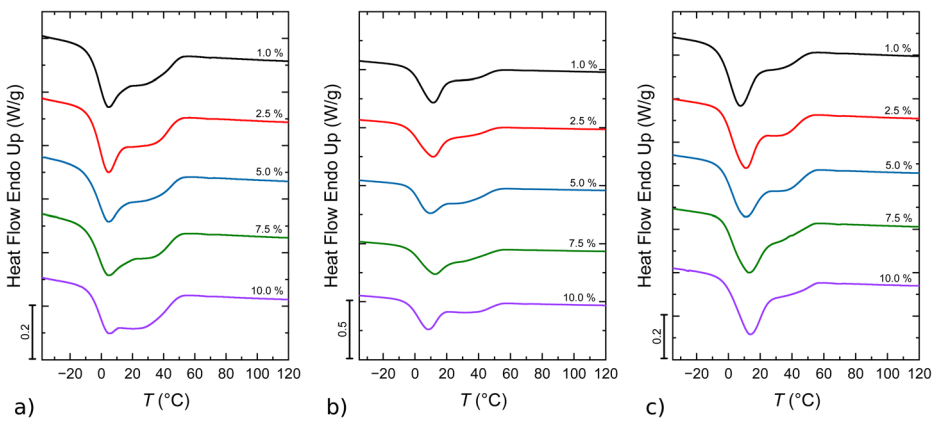

Fig. 2 DSC cooling curves at 20 °C min^{-1} of PBSA composites with (a) NdFeB, (b) SFO, and (c) SFO-CFO magnetic micro- and nanoparticles in the composition range of 1–10%.

© 2025 The Author(s). Published by the Royal Society of Chemistry

Open Access Article. Published on 15 2025. Downloaded on 02.11.2025 15:40:34.
This article is licensed under a Creative Commons Attribution-NonCommercial 3.0 Unported Licence.

as they all show unimodal melting endotherms. In the case of PBSA, a small cold crystallization exotherm is also observed during the DSC heating scans, which correlates with a reorganization process during the heating scan.[46]

The melting temperature (T_m) in polymers depends on the lamellar thickness, and because of the metastable nature of polymeric crystals (for kinetic reasons, usually polymers crystallize in thinner lamellae, which are considered metastable from a thermodynamic point of view, as the equilibrium crystalline structures should be lamellae with thickness equivalent to extended chain crystals), large changes in crystallization temperature (T_c) would be needed to modify the T_m values. So, it is usual to find that samples with or without nucleating agents exhibit similar T_m or with minimal changes. The observed T_m of ~56 °C for PCL and ~88 °C for PBSA homopolymers are consistent with the values reported in the literature.[15,20] Our PCL-based composites show relatively stable melting temperature values of 54.7–56.8 °C and PBSA-based composites of 84.8–87.6 °C largely independently of the type of filler particles, demonstrating that used M(N)Ps do not modify this parameter. The crystallinity degree (X_c) of the polymer in PMCs was evaluated, and the results are collected in Tables S1–S12.† As expected, the crystallinity degree did not change beyond the experimental error of the measurements. This suggests that the morphological structural features of the fillers employed here do not influence the crystallinity of the matrix in PMCs.

As explained above, it is worth underlining that M(N)Ps can act as nucleating agents. In particular, when the nucleation of added M(N)Ps is effective, a typical increase in crystallization temperature is detected, as the nucleation density is increased beyond that of the nucleating heterogeneities that the polymer already contains. To characterize this nucleating effect, the initial or "onset" crystallization temperature values ($T_{c,onset}$) was used. As shown in Fig. 3a, the $T_{c,onset}$ of the PMCs increases compared to the PCL homopolymer (in black), although it remains almost constant beyond 1% loading. In contrast, Fig. 3b shows a nearly linear increase in the $T_{c,onset}$ of PBSA-based PMCs with SFO (blue) and SFO-CFO (green) nanoparticles as their content increases. These variations are relatively low, and for $C > 10\%$, no significant changes in $T_{c,onset}$ were observed with increasing particle content (ESI, section S2†).

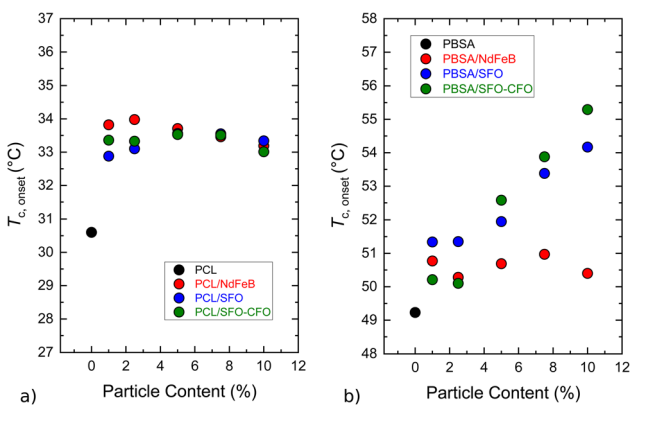

Fig. 3 $T_{c,onset}$ values of PMCs of (a) PCL and (b) PBSA with three types of M(N)Ps (NdFeB in red, SFO in blue, and SFO-CFO in green) in the filler content range of 1–10%.

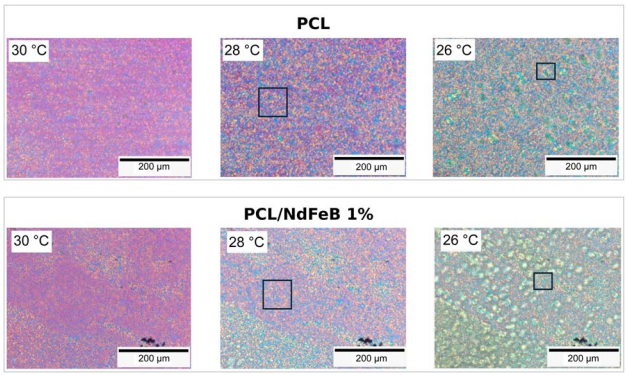

Fig. 4 PLOM micrographs of (upper panel) PCL homopolymer and (bottom panel) PCL/NdFeB composite ($C = 1\%$) at 30 °C, 28 °C, and 26 °C. Black boxes show differences in spherulitic average sizes between neat PCL *versus* the composite. In neat PCL, within the selected area of each box, the average spherulitic size is slightly larger.

3.2 Morphological properties

PLOM was employed to analyse the morphology as the samples were cooled from the melt. Fig. 4 compares the micrographs of PCL homopolymer and PCL/NdFeB composites ($C = 1\%$), recorded at different temperatures during cooling at 20 °C min^{-1}. Similar morphologies are observed for the homopolymer and the composite for a given temperature. In both cases, small spherulites are formed during crystallization, and there is no general evidence of the nucleating effect of the added M(N)Ps on the morphology of PCL. If the M(N)Ps were nucleating, they would be expected to create a higher number of nuclei, thereby decreasing the spherulitic size. However, localized regions of the micrographs, marked with black boxes in Fig. 4, reveal smaller spherulites in the composite compared to the neat PCL, indicating a nucleating effect limited to those areas. This morphological inhomogeneity is attributed to the poor dispersion of NdFeB microparticles in the sample. They tend to form aggregates,

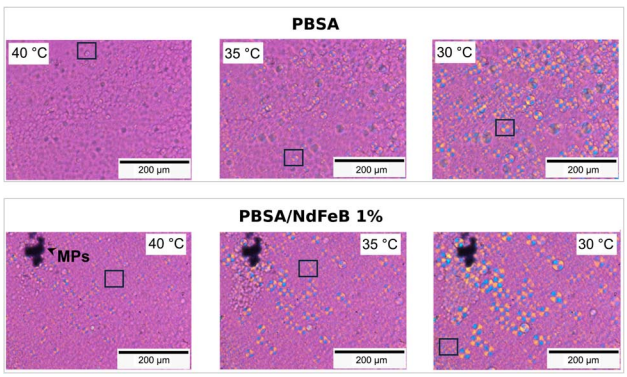

Fig. 5 PLOM micrographs of (upper panel) PBSA homopolymer and (bottom panel) PBSA/NdFeB 1% composite at 40 °C, 35 °C, and 30 °C. Black boxes show differences in spherulitic average sizes between neat PBSA *versus* the composite. In neat PBSA, within the selected area of each box, the average spherulitic size is slightly larger.

Open Access Article. Published on 15 2025. Downloaded on 02.11.2025 15:40:34.
This article is licensed under a Creative Commons Attribution-NonCommercial 3.0 Unported Licence.

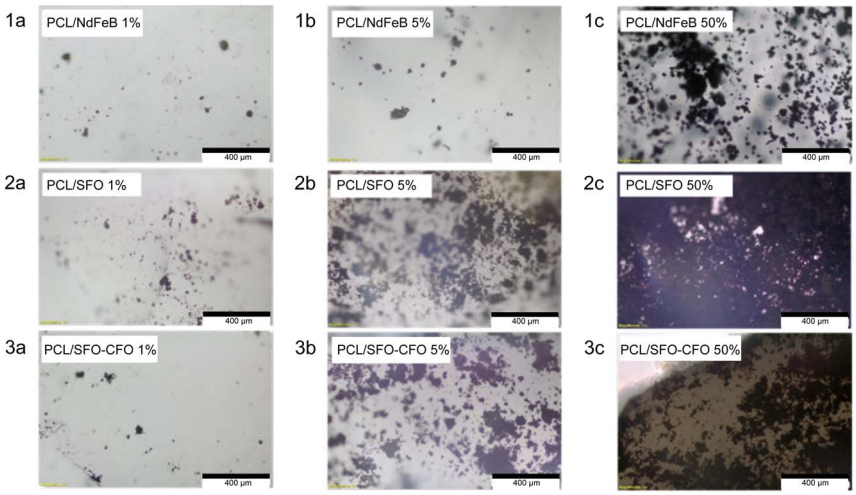

Fig. 6 PCM micrographs at room temperature of PCL-based composites: (1) PCL/NdFeB, (2) PCL/SFO, and (3) PCL/SFO-CFO, each at (a) 1%, (b) 5%, and (c) 50% filler content.

reducing their exposed surface area in contact with the PCL matrix, thus limiting their nucleating effect and resulting in the bimodal crystallization exotherms observed in Fig. S4.†

Micrographs of neat PBSA and PBSA/NdFeB (C = 1%) composites (Fig. 5), obtained during cooling at 20 °C min^{-1} from the melt, reveal a similar morphology. There is little evidence of a nucleating effect from the M(N)Ps, as shown by the PBSA homopolymer micrograph (Fig. 5 upper panel), where the formation of some spherulites at 40 °C is observed. However, in selected areas (shown by black boxes in Fig. 5), smaller spherulites can be observed in the composite *versus* the neat sample at the same crystallization temperature. In this case, the presence of M(N)Ps is also evident (see large black aggregates of M(N)Ps in the top left-hand corner of the image), and the dispersion is poor and non-homogenous, negatively affecting the nucleating effect of the M(N)Ps.

The morphology of selected samples was also examined using PCM at room temperature. Fig. 6 presents micrographs of PCL composites containing NdFeB, SFO, and SFO-CFO M(N)Ps at C = 1%, 5% and 50%. At 1% loading, the M(N)Ps form aggregates, indicating poor dispersion within the polymeric matrix. At 5% loading, many M(N)Ps are dispersed throughout the PCL matrix; however, aggregates are still clearly present. At 50% loading, the excessive M(N)P content leads to the formation of large aggregates within the polymer matrix, which likely diminishes the nucleating effect of the M(N)Ps. Similar observations were made using PCM for PBSA composites (Fig. S10†) with the same M(N)P loadings as those in the PCL composites. In the PBSA matrix, aggregates were also visible at low M(N)P contents, and the size and dispersion issues became more pronounced as the filler content increased.

4. Preliminary investigation of magnetic properties

SFO, SFO-CFO, and NdFeB M(N)Ps exhibit distinct magnetic properties, making them versatile fillers for PMCs. The maximum magnetization achievable under a given external field is critical for applications requiring strong magnetic responses, such as in 3D printing of functional materials, gears or magnetic actuators.[38,47,48] In the present case, magnetization at the maximum field of 2 T (M_{2T}) was measured. Coercivity ($\mu_0 H_C$), the resistance to demagnetization, is essential for magnetic stability in applications like patterned magnetic structures or memory devices, where precise and stable magnetic states are required.[26,28] The remanence ratio (M_R/M_{2T}) indicates how much magnetization is retained in the absence of an external field, which is crucial for applications like soft robotics or magnetic positioning systems that rely on residual magnetic forces for actuation.[49,50]

4.1 Magnetic properties of powders

The magnetic properties of the SFO, SFO-CFO, and NdFeB M(N)Ps, which reflect their potential for various polymer-based applications, were investigated by recording isothermal magnetization loops $M(H)$ in the $\mu_0 H = \pm 2$ T range (Fig. 7). NdFeB microparticles exhibit the highest magnetization ($M_{2T} \approx$ 84 Am^2 kg^{-1}), making them a strong candidate for applications in high-performance actuators or powerful magnetic composites used in energy harvesting or motors.[26,27,47,51] However, they possess a lower remanence ratio ($M_R/M_{2T} \approx 0.36$) and moderate coercivity ($\mu_0 H_C \approx 0.36$ T). It is important to underline that the values for NdFeB microparticles are obtained from a minor loop since the field of ±2 T was too low to saturate this sample. The characteristic feature of the minor loop is a vertical asymmetry of the hysteresis loop.[52] A kink in the low-field region of the hysteresis loop is also observed that has often been observed in NdFeB magnets and explained as the existence of soft magnetic phases due to damaged surface grains.[53] Notably, the general shape of the hysteresis loop and magnetic properties of these recycled microparticles match well with those reported in the literature for ~1 µm NdFeB particles with $\mu_0 H_C$ of ~0.32 T and M_R/M_{2T} of ~0.5.[54] The M_{2T} of our particles is ~20% lower,

© 2025 The Author(s). Published by the Royal Society of Chemistry

Open Access Article. Published on 15 2025. Downloaded on 02.11.2025 15:40:34.
This article is licensed under a Creative Commons Attribution-NonCommercial 3.0 Unported Licence.

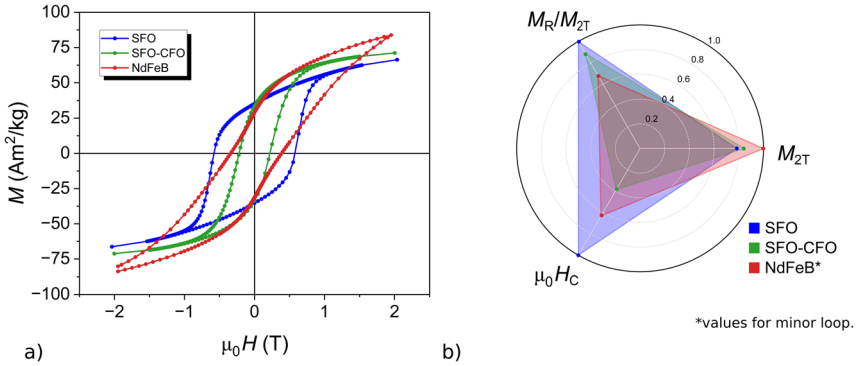

Fig. 7 (a) Field-dependent magnetization loops of M(N)Ps (SFO – blue, SFO-CFO – green, and NdFeB – red); (b) a radar diagram comparing the normalized magnetic properties of the powder samples. Note that a minor loop was recorded for the NdFeB powder. Each property—magnetization at 2 T (M_{2T}), remanence ratio (M_R/M_{2T}), and coercivity ($\mu_0 H_C$)—was normalized to the maximum value observed for that property across all samples. Measurements were performed at 300 K.

probably due to some epoxy resin that reduces the effective M(N)Ps mass fraction.

SFO nanoparticles, with their highest $\mu_0 H_C$ (~0.57 T), moderate M_{2T} (~66 Am^2 kg^{-1}), and high M_R/M_{2T} (~0.53), provide excellent magnetic remanence, making them suitable for patterned magnetic structures or permanent magnetic components in polymer matrices.[29,55,56] In contrast, SFO-CFO nanoparticles offer a balance between hard and soft magnetic behaviors, with slightly higher M_{2T} (~71 Am^2 kg^{-1}), moderate M_R/M_{2T} (~0.47), and low $\mu_0 H_C$ (~0.22 T). This combination makes SFO-CFO ideal for biomedical applications, such as magnetic hyperthermia or flexible magnetic sensors, where moderate magnetization and reconfigurability are critical.[21,22,57,58] Integrating these magnetic M(N)Ps into polymer matrices enables the creation of flexible, lightweight, and magnetically responsive composites.

4.2 Magnetic properties of composites

Fig. 8a presents the minor magnetization loops measured at 300 K for representative PCL-based composites with NdFeB microparticles with various filler contents C ranging from 1 to 90% (see additional plots in Fig. S11†). The $\mu_0 H_C$ varies non-monotonically between ~0.15 and 0.40 T, a behavior attributed to both the presence of soft magnetic phases in damaged grains and the inhomogeneous distribution of M(N)Ps within the polymer matrix. This distribution likely results in localized regions with distinct magnetic behaviors, contributing to the observed variability in coercivity.[59] The strong magnetic anisotropy of the NdFeB fillers prevented us to record hysteresis loops that reach saturation, even under an applied magnetic field of 2 T, making it challenging to evaluate the saturation magnetization of the composites accurately. Nonetheless, the measurements reveal that the M_{2T} increases proportionally with M(N)P content, as shown by the fit to the equation:

$$M_{2T}(C) = M_{powder}\left[\frac{C}{(100+C)}\right] = M_{powder}(w/100)$$

where C and w are the percentage filler loading and mass fraction, respectively (Fig. 8b).

To investigate the magnetic behavior in greater detail within the low-composition range (C = 1–10%), where the most significant changes (specifically step-like increase in $T_{c,onset}$ for PCL) in polymer properties were observed, field-dependent magnetization measurements were performed (Fig. 9). It should be underlined that the error on magnetization measurements is higher in this range due to errors in measuring the low masses of M(N)Ps. The SFO and SFO-CFO composites exhibit major magnetic hysteresis loops that saturate below 2 T. This behavior is consistent with the lower anisotropy of these ferrite-based materials compared to

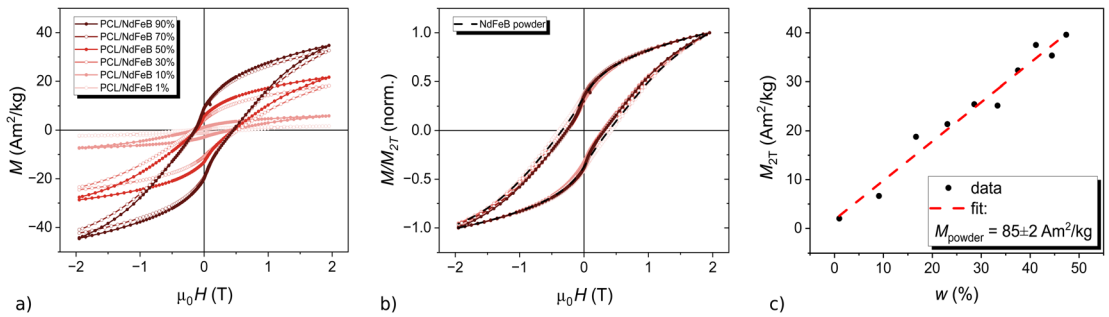

Fig. 8 (a) Field-dependent magnetization loops of PCL/NdFeB composites in the filler loading (C) range of 1–90% measured at 300 K (selected samples are shown); (b) the same curves normalized to magnetization measured at the applied field of 2 T (M_{2T}) and horizontally shifted to ease comparation with the pure powder (dashed black line); (c) M_{2T} as a function of filler mass fraction.

Open Access Article. Published on 15 2025. Downloaded on 02.11.2025 15:40:34.
This article is licensed under a Creative Commons Attribution-NonCommercial 3.0 Unported Licence.

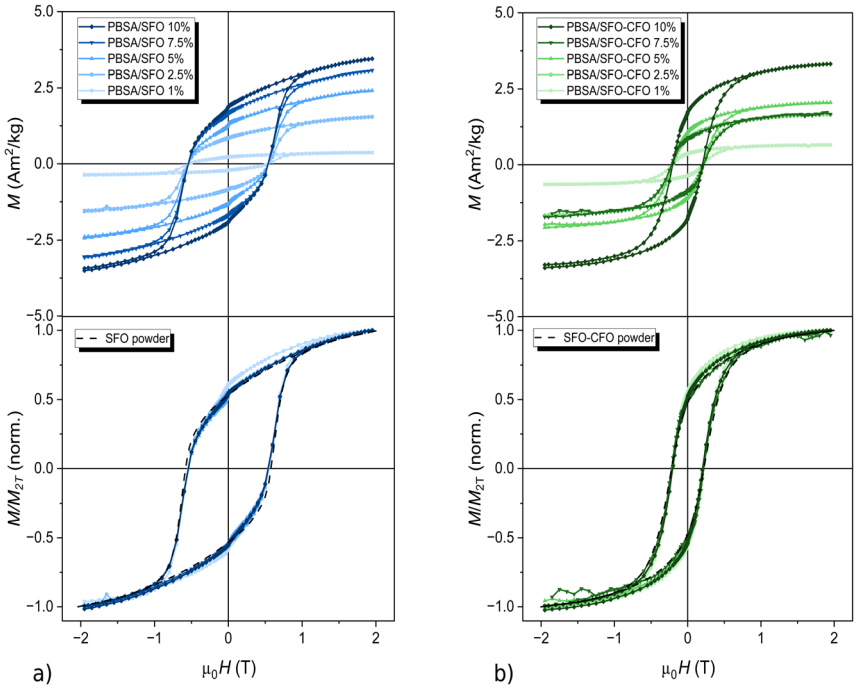

Fig. 9 Field-dependent magnetization loops of (a) SFO and (b) SFO-CFO PBSA-based composites normalized to entire mass (upper panel) and normalized to M_{2T} (bottom panel). All measurements were performed at 300 K.

NdFeB-based composites, which have higher anisotropy and thus require stronger fields for saturation. For PBSA/SFO composites, the M_R/M_{2T} ratio ranges from 0.54 to 0.59, while $\mu_0 H_C$ remains steady at ~0.53 T across the 1–10% filler loading range. In PBSA/SFO-CFO composites, the M_R/M_{2T} decreases from 0.56 at 1% to 0.51 at 10% and $\mu_0 H_C$ remains relatively stable at ~0.21 T. Overall, the magnetic properties of the PMCs are determined by the characteristics of the loaded M(N)Ps, so for NdFeB, which has the highest M_{2T} among the powders, the resulting composites also display the highest overall magnetization.

5 Conclusions

This work establishes that biodegradable polymer matrices combined with recycled NdFeB and REE-free lab-synthesized ferrite fillers exhibit controllable thermal and magnetic properties, with particle aggregation playing a dual role. Our findings indicate that magnetic particles can nucleate the polymer matrix during crystallization; however, aggregation limits this process, thereby maintaining the structural and thermal properties of the matrix. The magnetic properties of the PMCs closely reflect those of the embedded M(N)Ps, indicating that the particles largely preserve their intrinsic magnetic behavior even when dispersed in a polymer matrix. Notably, the M_R/M_{2T} and $\mu_0 H_C$ of the composites remain comparable to those of the pure particles, with only slight variations attributed to interparticle magnetic interactions and the polymer environment. This preservation of magnetic properties, combined with the tunable magnetic response through filler concentration, highlights the potential of these PMCs for various applications.

This preliminary study offers a promising framework to develop these materials further, opening perspectives for applications in sustainable technologies. Refining particle dispersion strategies appears to be a key point to improve the material's performance. Finally, investigating multi-component systems could further enhance their performance and expand their functionality.

Abbreviations

PMCs	Polymer-based magnetic composites
M(N)Ps	Micro- or nanoparticles
PCL	Poly(ε-caprolactone)
PBSA	Poly(butylene succinate-*ran*-butylene adipate)
PLA	Poly(lactic acid)
REE	Rare earth elements
NdFeB	Neodymium–iron–boron alloy
SFO	Strontium ferrite
SFO-CFO	Strontium ferrite/cobalt ferrite
DSC	Differential scanning calorimetry
PLOM	Polarized light optical microscopy
PCM	Phase contrast microscopy
VSM	Vibrating sample magnetometry

Data availability

The data supporting the findings of this study are available within the article and its ESI.† There is no code used in this study. Additional data are available from the corresponding authors on reasonable request.

© 2025 The Author(s). Published by the Royal Society of Chemistry

Open Access Article. Published on 15 2025. Downloaded on 02.11.2025 15:40:34.
This article is licensed under a Creative Commons Attribution-NonCommercial 3.0 Unported Licence.

Author contributions

Ayda Ghary Haghighat: investigation, visualization. Eider Matxinandiarena: investigation, methodology, data curation, visualization, writing – original draft. Manuela Zubitur: investigation, formal analysis, writing – original draft. Agurtzane Mugica: investigation, formal analysis, validation. Fulvio Bellato: methodology, investigation, validation. Anna M. Ferretti: methodology, investigation, writing – original draft. Alessandro Ponti: methodology, investigation, validation, writing – review & editing. Souad Ammar: investigation, resources, writing – review & editing. Maryam Abdolrahimi: investigation, formal analysis. Gaspare Varvaro: conceptualization, resources, supervision, writing – review & editing. Pierfrancesco Maltoni: investigation, methodology, validation, writing – original draft. Dario Cavallo: investigation, formal analysis, validation, writing – review & editing. Alexander Omelyanchik: investigation, data curation, methodology, visualization, writing – original draft, writing – review & editing. Alejandro J. Müller: investigation, conceptualization, methodology, supervision, writing – review & editing, resources, funding acquisition. Davide Peddis: investigation, conceptualization, methodology, supervision, writing – original draft, writing – review & editing, resources, project administration, funding acquisition.

Conflicts of interest

There are no conflicts to declare.

Acknowledgements

This work has been partially supported by the project Recycling End-of-Life Permanent Magnets by Innovative Sintering and 3D Printing (RENDERING 3D) granted within the framework of the call ERAMIN 2022. The UniGe and CNR teams acknowledge partial support by the project Circular economy of rare-earth permanent magnets (ReCREATE) granted by ICO-FALCK Foundation through Politecnico di Milano Foundation. The UPV/EHU team acknowledges funding from: (1) MICIU/AEI/10.13039/501100011033 and "European Union NextGenerationEU/PRTR" of the grant PCI2022-132942; (2) María de Maeztu Excellence Unit CEX2023-001303-M funded by MCIN/AEI/10.13039/501100011033; and (3) The Basque Government through grant IT1503-22.

References

1 V. K and A. Tiwari, *Inorg. Nano-Met. Chem.*, 2023, 1–25.
2 Y. Kim and X. Zhao, *Chem. Rev.*, 2022, **122**, 5317–5364.
3 E. M. Palmero and A. Bollero, *3D and 4D Printing of Functional and Smart Composite Materials*, Elsevier Ltd., 2021, vol. 2.
4 K. G and B. Kandasubramanian, *Ind. Eng. Chem. Res.*, 2022, **61**, 16895–16909.
5 C. Zhang, X. Li, L. Jiang, D. Tang, H. Xu, P. Zhao, J. Fu, Q. Zhou and Y. Chen, *Adv. Funct. Mater.*, 2021, **31**(34), DOI: **10.1002/adfm.202102777**.
6 A. Amirov, A. Omelyanchik, D. Murzin, V. Kolesnikova, S. Vorontsov, I. Musov, K. Musov, S. Khashirova and V. Rodionova, *Processes*, 2022, **10**, 2412.
7 A. Makridis, N. Okkalidis, D. Trygoniaris, K. Kazeli and M. Angelakeris, *J. Phys. D Appl. Phys.*, 2023, **56**, 285002.
8 A. Zimina, A. Nikitin, V. Lvov, I. Bulygina, P. Kovaleva, S. Vodopyanov, M. Zadorozhnyy, E. Peshkina, S. Karshieva, R. Choudhary, M. Abakumov and F. Senatov, *J. Compos. Sci.*, 2024, **8**, 48.
9 I. Galarreta-Rodriguez, A. Lopez-Ortega, E. Garayo, J. J. Beato-López, P. La Roca, V. Sanchez-Alarcos, V. Recarte, C. Gómez-Polo and J. I. Pérez-Landazábal, *Adv. Compos. Hybrid Mater.*, 2023, **6**, 102.
10 M. B. Lodi, A. Makridis, N. M. Carboni, K. Kazeli, N. Curreli, T. Samaras, M. Angelakeris, G. Mazzarella and A. Fanti, *IEEE Access*, 2022, **10**, 19768–19779.
11 L. Zárybnická, M. Pagáč, R. Ševčík, J. Pokorný and M. Marek, *Magnetochemistry*, 2023, **9**, 232.
12 M. E. Pekdemir, D. Aydin, S. Selçuk Pekdemir, P. Erecevit Sönmez and E. Aksoy, *J. Inorg. Organomet. Polym. Mater.*, 2023, **33**, 1147–1155.
13 A. Cheremnykh, P. Kovaleva, I. Bulygina, A. Korol, I. Krupatin, A. Nikitin, E. Statnik and F. Senatov, *Mater. Lett.*, 2024, **372**, 137045.
14 R. B. Kristiawan, F. Imaduddin, D. Ariawan, U. Ubaidillah and Z. Arifin, *Open Eng.*, 2021, **11**, 639–649.
15 G. Ö. Kayan and A. Kayan, *ChemEngineering*, 2023, **7**, 104.
16 L. Aliotta, M. Seggiani, A. Lazzeri, V. Gigante and P. Cinelli, *Polymer*, 2022, **14**, 844.
17 M. Puchalski, G. Szparaga, T. Biela, A. Gutowska, S. Sztajnowski and I. Krucińska, *Polymer*, 2018, **10**, 251.
18 T. Zhao, J. Yu, X. zhang, W. Han, S. zhang, H. Pan, Q. Zhang, X. Yu, J. Bian and H. Zhang, *Polym. Bull.*, 2024, **81**, 2481–2504.
19 H. Emadi, M. Karevan, M. Masoudi Rad, S. Sadeghzade, F. Pahlevanzadeh, M. Khodaei, S. Khayatzadeh and S. Lotfian, *Polymer*, 2023, **15**, 3617.
20 N. Thummarungsan and A. Sirivat, *J. Polym. Environ.*, 2024, **32**, 3246–3257.
21 G. Zhu, Y. Hou, N. Xia, X. Wang, C. Zhang, J. Zheng, D. Jin and L. Zhang, *Adv. Funct. Mater.*, 2023, **33**, 1–12.
22 L. Du, Z. Y. Xu, C. J. Fan, G. Xiang, K. K. Yang and Y. Z. Wang, *Macromolecules*, 2018, **51**, 705–715.
23 G. Wang, S. Yang, Z. Wei, X. Dong, H. Wang and M. Qi, *Polym. Bull.*, 2013, **70**, 2359–2371.
24 W. Sas, M. Jasiurkowska-delaporte, P. Czaja, P. M. Zieliński and M. Fitta, *Magnetochemistry*, 2021, **7**, 1–10.
25 H. Deng, K. Sattari, Y. Xie, P. Liao, Z. Yan and J. Lin, *Nat. Commun.*, 2020, **11**, 1–10.
26 K. Tao, J. Wu, A. G. P. Kottapalli, D. Chen, Z. Yang, G. Ding, S. W. Lye and J. Miao, *Solid State Electron.*, 2017, **138**, 66–72.
27 K. von Petersdorff-Campen, Y. Hauswirth, J. Carpenter, A. Hagmann, S. Boës, M. Schmid Daners, D. Penner and M. Meboldt, *Appl. Sci.*, 2018, **8**, 1275.
28 J. Wang, H. Xie, L. Wang, T. Senthil, R. Wang, Y. Zheng and L. Wu, *J. Alloys Compd.*, 2017, **715**, 146–153.

Open Access Article. Published on 15 2025. Downloaded on 02.11.2025 15:40:34. This article is licensed under a Creative Commons Attribution-NonCommercial 3.0 Unported Licence.

29 P. Ershov, V. Salnikov, P. Vorontsov, A. Omelyanchik, A. Amirov, A. Zhansitov, K. Musov, S. Khashirova, F. Senatov, Y. Raikher and V. Rodionova, *Mater. Lett.*, 2025, **382**, 137913.
30 K. Schäfer, T. Braun, S. Riegg, J. Musekamp and O. Gutfleisch, *Mater. Res. Bull.*, 2023, **158**, 112051.
31 A. Becci, F. Beolchini and A. Amato, *Processes*, 2021, **9**, 857.
32 R. Schulze and M. Buchert, *Resour. Conserv. Recycl.*, 2016, **113**, 12–27.
33 Y. Yang, A. Walton, R. Sheridan, K. Güth, R. Gauß, O. Gutfleisch, M. Buchert, B. M. Steenari, T. Van Gerven, P. T. Jones and K. Binnemans, *J. Sustain. Metall.*, 2017, **3**, 122–149.
34 A. Amato, A. Becci, A. Bollero, M. del M. Cerrillo-Gonzalez, S. Cuesta-Lopez, S. Ener, I. Dirba, O. Gutfleisch, V. Innocenzi, M. Montes, K. Sakkas, I. Sokolova, F. Vegliò, M. Villen-Guzman, E. Vicente-Barragan, I. Yakoumis and F. Beolchini, *ACS Sustain. Chem. Eng.*, 2023, **11**, 13374–13386.
35 C. Huber, M. Goertler, C. Abert, F. Bruckner, M. Groenefeld, I. Teliban and D. Suess, *Sci. Rep.*, 2018, **8**, 1–8.
36 C. Huber, C. Abert, F. Bruckner, M. Groenefeld, O. Muthsam, S. Schuschnigg, K. Sirak, R. Thanhoffer, I. Teliban, C. Vogler, R. Windl and D. Suess, *Appl. Phys. Lett.*, 2016, **109**, 162401.
37 L. Pigliaru, M. Rinaldi, L. Ciccacci, A. Norman, T. Rohr, T. Ghidini and F. Nanni, *Funct. Compos. Mater.*, 2020, **1**, 1–18.
38 M. B. Khan, K. Schäfer, F. Hofmann, M. Lutzi, E. S. Oliveros-Mata, O. Pylypovskyi, D. Makarov and O. Gutfleisch, *Adv. Intell. Syst.*, 2024, 1–10.
39 R. C. Pullar, *Prog. Mater. Sci.*, 2012, **57**, 1191–1334.
40 P. Maltoni, T. Sarkar, G. Barucca, G. Varvaro, F. Locardi, D. Peddis and R. Mathieu, *J. Phys. Chem. C*, 2021, **125**, 5927–5936.
41 P. Maltoni, T. Sarkar, G. Barucca, G. Varvaro, D. Peddis and R. Mathieu, *J. Magn. Magn. Mater.*, 2021, **535**, 168095.
42 P. Maltoni, T. Sarkar, G. Varvaro, G. Barucca, S. A. Ivanov, D. Peddis and R. Mathieu, *J. Phys. D Appl. Phys.*, 2021, **54**, 124004.
43 P. Maltoni, G. Barucca, B. Rutkowski, M. C. Spadaro, P. E. Jönsson, G. Varvaro, N. Yaacoub, J. A. De Toro, D. Peddis and R. Mathieu, *Small*, 2024, **20**(10), 2304152.
44 J. M. Schultz, Polymer crystallization, *The Development of Crystalline Order in Thermoplastic Polymers*, Oxfrod University Press, Oxford, U.K., 2001.
45 D. Cavallo and A. J. Müller, in *Macromolecular Engineering: from Synthesis to Macroscopic Materials and Applications*, ed. K. Matyjaszewski, Y. Gnanou, N. Hadjichristidis and M. Muthukumar, Wiley, Second., 2022, pp. 1–57.
46 I. Arandia, A. Mugica, M. Zubitur, A. Arbe, G. Liu, D. Wang, R. Mincheva, P. Dubois and A. J. Müller, *Macromolecules*, 2015, **48**, 43–57.
47 M. Ferrara, M. Rinaldi, L. Pigliaru, F. Cecchini and F. Nanni, *J. Appl. Polym. Sci.*, 2022, **139**(20), 52150.
48 G. Chatzipirpiridis, S. Gervasoni, C. Fischer, O. Ergeneman, E. Pellicer, B. J. Nelson and S. Pané, *Adv. Intell. Syst.*, 2019, **1**, 1900069.
49 V. Iacovacci, G. Lucarini, C. Innocenti, N. Comisso, P. Dario, L. Ricotti and A. Menciassi, *Biomed. Microdevices*, 2015, **17**, 1–7.
50 E. S. Oliveros-Mata, R. Xu, L. Guo and D. Makarov, *Phys. Rev. Appl.*, 2023, **20**, 060501.
51 L. A. Makarova, Y. A. Alekhina, D. A. Isaev, M. F. Khairullin and N. S. Perov, *J. Phys. D Appl. Phys.*, 2021, **54**, 015003.
52 J. Huang, X. Liu, X. Kan, S. Feng, Y. Yang, Q. Lv, C. Liu, J. Zhao and M. Shezad, *J. Mater. Sci. Mater. Electron.*, 2020, **31**, 20325–20331.
53 S. E. Ilse, F. Groß, G. Schütz, J. Gräfe and E. Goering, *Phys. Rev. B*, 2021, **103**, 24425.
54 H. Guo, H. Zhang, W. Li, R. Jiang, X. Liang and X. Zhou, *Eur. Polym. J.*, 2024, **213**, 113116.
55 T. Hanemann, D. Syperek and D. Nötzel, *Materials*, 2020, **13**, 1–13.
56 F. Yang, X. Zhang, Z. Guo, S. Ye, Y. Sui and A. A. Volinsky, *J. Alloys Compd.*, 2019, **779**, 900–907.
57 M. Lalegani Dezaki and M. Bodaghi, *Int. J. Adv. Manuf. Technol.*, 2023, **126**, 35–48.
58 R. Xu, G. S. Cañón Bermúdez, O. V. Pylypovskyi, O. M. Volkov, E. S. Oliveros Mata, Y. Zabila, R. Illing, P. Makushko, P. Milkin, L. Ionov, J. Fassbender and D. Makarov, *Nat. Commun.*, 2022, **13**, 6587.
59 E. Y. Kramarenko, A. V Chertovich, G. V Stepanov, A. S. Semisalova, L. A. Makarova, N. S. Perov and A. R. Khokhlov, *Smart Mater. Struct.*, 2015, **24**, 035002.

© 2025 The Author(s). Published by the Royal Society of Chemistry